Instituts für Organische Chemie der Freien Universität Berlin. Thermal analyses were carried out on a differential scanning calorimeter (Perkin-Elmer DSC-2C). Surface tension was measured with an interfacial tensiometer (Krüss) by the du Noüy ring detachment method. Electron micrography was performed on a Philips EM-400T electron microscope.

1,1″-[(1,18-Dioxo-1,18-octadecanediyl)bis(oxy-11,1-undecanediyl)]-bis[1′-methyl-4,4′-bipyridinium] Tetrachloride (3c). Octadecanedioic acid (4.5 g, 14.3 mmol) was dissolved in 50 mL of thionyl chloride and refluxed for 5 h. The solvent was removed, and the resulting octadecanedioyl dichloride dissolved in 50 mL of dry chloroform. This solution was added dropwise to a stirred solution of 7.19 g (28.6 mmol) 11-bromo-1-undecanol in 50 mL of dry chloroform containing 3.3 mol (28.6 mmol) of 2,6-lutidine at 0 °C. After 30 min at 0 °C the solution was stirred for 3 h at room temperature. The solvent was removed and the residue extracted 5 times with hot hexane (~1 L). The combined extracts were decolorized with alumina; and the solvent was evaporated to 500 mL. Crystallization at 0 °C yielded 7.3 g (66%) of white microcrystals of octadecanedioic acid bis(11-bromoundecyl) ester (mp 58 °C).

This α,ω-dibromo ester (6.0 g, 7.7 mmol) was refluxed for 3.5 h in nitromethane with 7.2 g (46 mmol) of 4,4′-bipyridine. After cooling to room temperature the product precipitated and was recrystallized from *n*-butanol, yielding 6.4 g (76%) of white platelets (mp 131–133 °C).

This bis(bipyridinium) salt (5.4 g, 4.9 mmol) was dissolved in 100 mL of nitromethane at 60 °C. An excess (1.4 mL, 15 mmol) of dimethyl sulfate was added and stirred for 3.5 h at 60 °C. After standing overnight at room temperature it was cooled in an ice bath. The crude product precipitated. It was redissolved in methanol and filtered over Amberlite C 64001 to give the tetrachloride **3c** after two crystallizations from methanol. Yielding 3.5 g (65%) of slightly yellow-brown microcrystals: mp >250 °C; ^{1}H NMR (CD_3OD) δ 9.30 (d, 4 H), 9.20 (d, 4 H), 8.68 (m, 8 H), 4.75 (t, 4 H), 4.53 (s, 6 H), 4.05 (t, 4 H), 2.30 (t, 4 H), 2.10 (m, 4 H), 1.61 (m, 8 H), 1.32 (m, 52 H); UV max 259 nm (ϵ 39400). Anal. Calcd for $C_{62}H_{98}Cl_4N_4O_4$: C, 67.37; H, 8.94; N, 5.07. Found: C, 66.9; H, 9.0; N, 4.7.

1,1″-[(1,18-Dioxo-1,18-octadecanediyl)bis(oxy-11,1-undecanediyl)]-bis[1′-methyl-4,4′-bipyridinium] Tetraperchlorate (3d). A concentrated methanolic solution of **3c** was mixed with an excess of lithium perchlorate in methanol. **3d** precipitated and was recrystallized from methanol/ethanol.

Anal. Calcd for $C_{62}H_{98}Cl_4N_4O_{20}$: C, 54.70; H, 7.26; N, 4.12. Found: C, 54.64; H, 7.28; N, 4.13.

Typical vesicle formation involved the dissolution of **3c** in distilled water (10^{-3} M) and titration with sodium perchlorate solution. After addition of 1 equiv of this salt the solution became slightly turbid. To separate a water-soluble porphyrin[5] from vesicles made from **3e** a G 50 Sephadex column (h = 20 cm, ϕ = 1 cm) was used. This was first saturated with the tetrachloride **3c** and washed with distilled water. The vesicles containing the porphyrin in the inner water volume separated in a sharp band from the free porphyrin on such presaturated columns. Without presaturation[15] the vesicle fraction smeared over the whole column.

Electron micrographs were taken after adsorbing the amphiphilic aggregates on a carbon film (thickness 40 Å), applying a gentle procedure of freeze-drying and tungsten shadowing.[16] The length of sharply delineated shadows (e.g., Figure 3a) of latex particles was taken as a measure for the thickness of the crystals and micelles. Negative staining with uranylacetate was also performed on the same carbon films.

Acknowledgment. Support of this work by the Deutsche Forschungsgemeinschaft, the Fonds der Chemischen Industrie, and the Förderungskommission für Forschung und wissenschaftlichen Nachwuchs der Freien Universität Berlin is gratefully acknowledged (FGS Biomembranen). We also thank Dipl.-Chem. Gustav Penzlin for a drawing.

Registry No. 3a, 88888-76-0; **3b**, 88904-46-5; **3c**, 88888-77-1; **3d**, 88888-79-3; **3e**, 88888-80-6; **3f**, 88904-47-6; bis(11-pyridinioundecyl)-octadecanedioate dibromide, 88888-81-7.

(15) Huang, C.-H. *Biochemistry* **1969**, *8*, 344.
(16) Tesche, B. *Mikroskopie* **1978**, *34*, 29.

A One-Dimensional Polymeric Ribbon Alternative to the Aggregation of d^8 ML_4 Fragments

Roald Hoffmann,*† Christian Minot,† and Harry B. Gray‡

Contribution from the Department of Chemistry, Cornell University, Ithaca, New York 14853, and the Arthur Ames Noyes Laboratory, California Institute of Technology, Pasadena, California 91125. *Received July 12, 1983*

Abstract: d^8 ML_4 fragments normally trimerize, as in $Os_3(CO)_{12}$, or stack, as in $Pt(CN)_4^{2-}$. There is an alternative to these aggregation modes. Still unobserved, but not unreasonable, is the formation of a one-dimensional infinite ribbon, stoichiometry ML_2X, with X bridging and a zigzag single-bonded metal chain, **6**. The detailed analysis of the band structure of this material is the subject of this work.

Think about the d^8 ML_4 fragment. Two geometries are likely for it, the angular **1**, an octahedron minus two cis ligands, and the flat **2**, an octahedron minus two trans ligands. If one examines the possible realizations of this fragment, from Fe, Ru, Os(0) through Co, Rh, Ir(I) to Ni, Pd, Pt(II), and Cu, Ag, Au(III), one realizes that the angular **1** is favored for low oxidation states and the flat **2** for the more electronegative high oxidation states of the late transition metals. The reasons for this preference are reasonably well understood (see Appendix).

A further difference emerges between the angular and flat fragments if we think about their kinetic and/or thermodynamic stability. **1** is not stable, but typically trimerizes to **3**, as for $Os_3(CO)_{12}$.[1] **2** is usually kinetically and thermodynamically stable

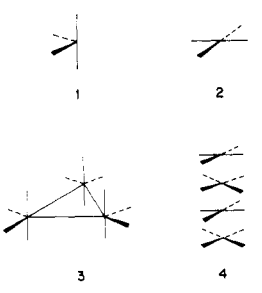

as the monomer, e.g., $Pt(CN)_4^{2-}$. But for certain square-planar d^8 complexes there is a definite tendency to one-dimensional

† Cornell University.
‡ California Institute of Technology.

(1) Corey, E. R.; Dahl, L. F. *Inorg. Chem.* **1962**, *1*, 521–526. For $Ru_3(CO)_{12}$ see: Mason, R.; Rae, A. I. M. *J. Chem. Soc. A* **1978**, 778–779.

0002-7863/84/1506-2001$01.50/0

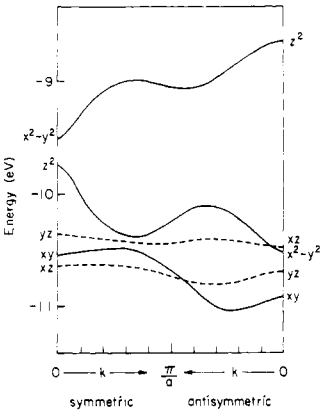

Figure 1. The energy bands of $[RuCl_3^-]_\infty$. The bands are unfolded so that the levels symmetric with respect to the screw axis are at the left and those antisymmetric are at the right. There is an avoided crossing of x^2-y^2 and z^2 bands at the left side of the figure.

aggregation of type **4**, in solution and in the solid state.[2] We suggest that an interesting and apparently not yet observed aggregation alternative to **3** is available to the angular fragment **1**. This is **5** or its sterically more confortable realization **6**, both infinite one-dimensional chains.

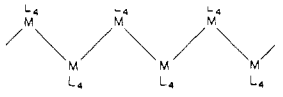

5

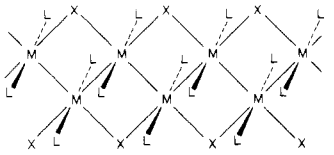

6

The stoichiometry of **6** is ML_2X. If X is a halide and L a neutral base then the 18-electron count at the metal is achieved for M = Co, Rh, Ir(I). This paper is concerned with the electronic structure of these hypothetical one-dimensional systems.

If we assume reasonable MM (3.0 Å) and MX (2.5 Å) distances, we still have two degrees of freedom in the angles. Calculations were carried out at several assumed angles, but only those for MMM = 75.7° and MMX = MXM = 94.8° are reported here. The polymer is schematized in **7**. Note an important

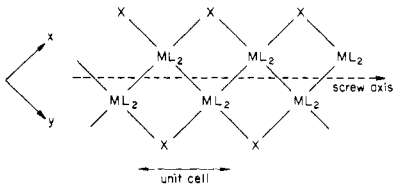

7

screw axis or glide line, which will figure significantly in the subsequent discussion. The unit cell contains two ML_2X units.

The band structure of a hypothetical $(RuCl_3^-)_\infty$ is shown in Figure 1.[3] All the levels may be classified as symmetric or

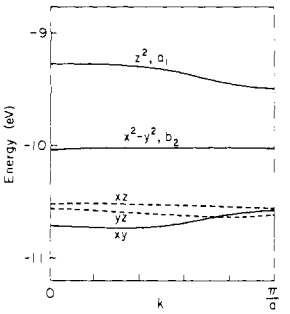

Figure 2. The band structure of the $[RuCl_3^-]_\infty$ "half-polymer", **9**.

antisymmetric with respect to the screw axis everywhere in the Brillouin zone. This allows an alternative representation, "unfolding" the bands so as to group all the antisymmetric bands after the symmetric ones. This is done at the right in Figure 1.

How are we to understand, as chemists, these band structures? We could focus on the three below two splitting which we would expect at each octahedral center. Indeed this allows us at once to see the partitioning between the three lower bands of Figure 1, which are derived from the t_{2g} level and are not very broad, and the two upper bands. But to see the essence of metal–metal bonding requires a different viewpoint.

Recall the orbitals of an ML_4 fragment **8**.[4] Above the t_{2g} set is an out-of-phase combination of two directed hybrids, a mixture of p_x, p_y, and x^2-y^2, b_2. Still higher is the a_1 hybrid, a mixture of s, p_x, p_y, x^2-y^2, and substantial z^2. Now a relatively "harmless"

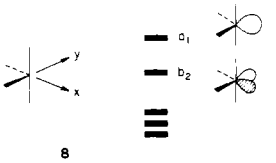

8

(to the electronic structure) assembly of these fragments is the hypothetical polymer **9**, "half" of our intended structure. Its band structure is shown in Figure 2. Note that none of the bands acquire great dispersion. Neither the "t_{2g}" orbitals nor the a_1 and b_2 hybrids interact much.

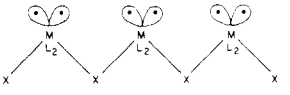

9

Very different things happen for the hybrids a_1 and b_2 when two chains of **9** are put together. The "a_1"- and "b_2"-derived bands are of high dispersion. Obviously the hybrids on one chain interact with those of another. Let us dissect the interactions in detail.

For one chain of type **9** the a_1 hybrids form a band with k = 0 (all in-phase combination) being **10a** and the $k = \pi/a$ (all out-of-phase combination) being **10b**. These now combine to give

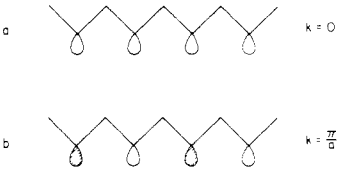

10

four combinations, **11**. It is very easy to decide whether these

(2) (a) Miller, J. S., Ed. "Extended Linear Chain Compounds"; Plenum: New York, 1982; Vol. 1–3. (b) Miller, J. S.; Epstein, A. J. *Prog. Inorg. Chem.* **1976**, *20*, 1–151.

(3) The calculations are extended Hückel band calculations. A description of the method is given by Whangbo and Hoffmann: [Whangbo, M.-H.; Hoffmann, R. *J. Am. Chem. Soc.* **1978**, *100*, 6093–6098] and the computational parameters are listed in the Appendix.

(4) See: Elian, M.; Hoffmann, R. *Inorg. Chem.* **1975**, *14*, 1058–1076 and references therein.

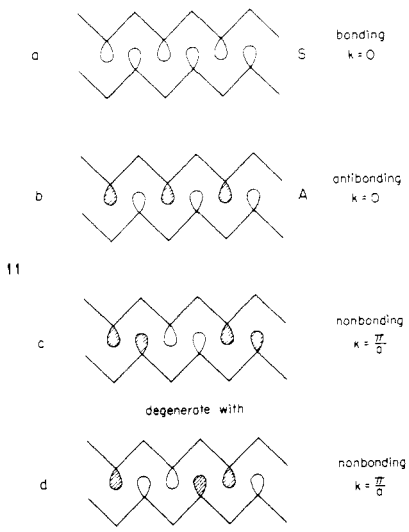

11

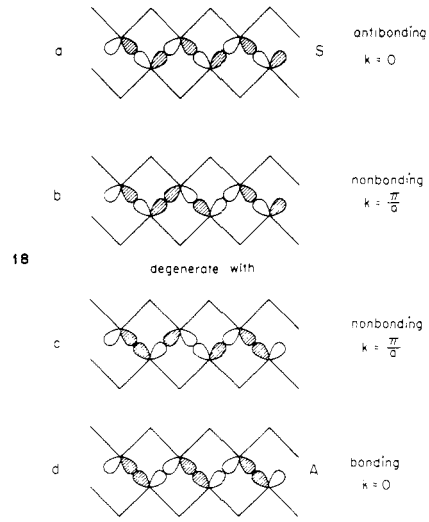

18

combinations are bonding or antibonding and to classify them according to the polymer screw axis. The qualitative conclusion as to the shape of the band that results, expressed in the notation of Figure 1b, is as follows, **12**. Alternatively one could begin with

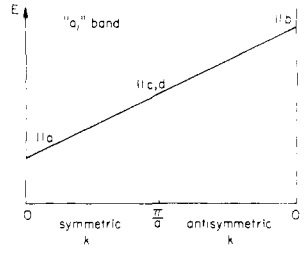

12

the two orbitals of the unit cell, **13**, split them as bonding **14** or antibonding **15**, and then develop bands from them. In fact let

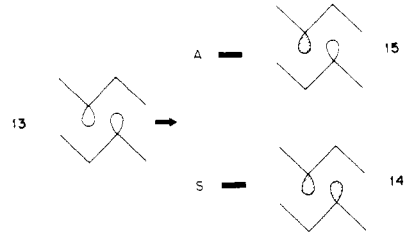

us now follow this second approach for the bands derived from the b_2 orbitals of the fragment. The unit cell combinations are shown in **16** and **17** Note the screw axis symmetries differ from

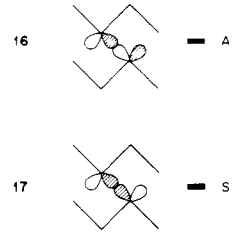

14 and **15**. Now the translational symmetry develops each into a band. **18** shows the top and bottom orbitals of each band. Plotted out in the notation of Figure 1 the slope of this band would be just opposite in sign to that of the a_1 band.

Superimposed on this is the fact that the center of gravity of the b_2 band is below the a_1 band, or to put it in another way, in the ML_4 fragment b_2 is below a_1. It follows that the anticipated band structure is that of **19**:

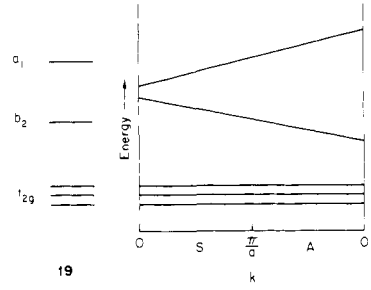

19

How does this idealized picture compare to the actual band structure of Figure 1? Really quite well—the differences are explained next. First of all the band derived from b_2 has the same symmetry in the interior of the Brillouin zone as a band derived from one member of the t_{2g} set. This leads to an obvious avoided crossing near the middle of the diagram and the undulations at right. Second the bottom of the band derived from a_1 emerges below the top of the b_2 band, both at $k = 0$. This implies another avoided crossing at small k values on the left side of the diagram. Other than these details the general features of **19** are preserved in the band structure.

Let us turn to the metal–metal bonding. The three lowest levels generate three flat bands, occupied for a d^6 electron count. Completely filled are both the MM bonding and the MM antibonding combinations of orbitals, so that the net contribution to MM bonding is nil.

The same thing, no metal–metal bonding, would seem to be implied for a d^8 count, in which the band derived from b_2 would be filled. To see this look at **18**. The bottom of the band (A, $k = 0$; bonding), the middle (S, $k = \pi/a$; A, $k = \pi/a$; nonbonding), and the top (S, $k = 0$; antibonding) all are filled. Net MM bonding should be small. Yet a simple chemical picture, one we started out with near the beginning, would lead us to expect MM bonding for a d^8 complex. The simple picture should be right, so let us see how the interpretation of the band structure needs to be modified to come into correspondence with simple electron counting.

Suppose we had taken a different starting point for our band construction, that of localized metal–metal σ and σ^* bonds, **20** and **21**. Forgetting the true symmetry of the polymer, let us just

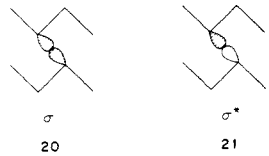

20 21

"spread out into a band" the σ levels. The zone center "k" = 0

is then **22**, the zone edge is **23**. A similar construction, not shown

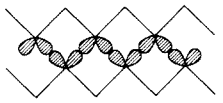

22

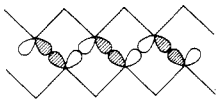

23

here, may be made for the σ^* band. The reason that k appears in quotation marks above is that this process of band formation really corresponds to idealized delocalization in a linear metal chain, **24a**, rather than the true zigzag one, **24b**. Or to put it another way, we have turned to the true electronic repeat unit,

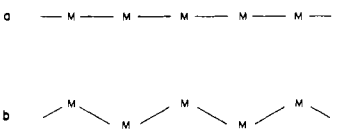

24

which is one metal atom (or one metal–metal bond) rather than two. Something very similar occurs in considerations of polyacetylenes. $(CH)_n$, where the true repeat unit in a realistic trans geometry is two carbons, but the basic electronic unit is one carbon long.[5]

Let us return to the "localized" construction band, the extremes of which are shown in **22** and **23**. We would all agree that filling that band with two electrons per bond would give a single metal–metal bond. But now think about the relationship of this band to the bands previously constructed from a_1 and b_2 levels. It is clear that **22** is like **11a**, the $k = 0$ point of the a_1 band, and that **23** is like **18d**, the $k = \pi/a$ point of the b_2 band. We thus jump to the following generalization: to obtain metal–metal bonding it is necessary to fill the a_1 band instead of the b_2 band in the region symmetric with respect to the screw axis (thus replacing antibonding interactions by bonding ones).

The orbitals perform this transformation naturally for us. At the left of Figure 1, the region symmetric with respect to the symmetry axis, the a_1 and b_2 bands come close together. At $k = 0$ they cannot mix by symmetry, and with this choice of parameters the combination derived from the a_1 actually is lower than the top of the b_2 band. The moment one departs from the zone center the a_1 and b_2 derived bands mix and do so strongly. Notice the fourth and fifth band "repelling" each other at the left in Figure 1. Figure 3 shows the actual populations in the HOMO of a d^8 polymer, the fourth band from the bottom in Figure 1, of the main component of a_1, which is z^2, and of the main component of b_2, which is x^2-y^2 in our coordinate system. The left side of the band is mainly z^2 and the right side of the band mainly x^2-y^2. So the conditions for metal–metal σ bonding have come about.

Another way to look at this phenomenon is to examine the MM overlap population for a d^8 polymer at different k points. The original simplified model which we described above would lead one to expect antibonding on the left-hand side of the Brillouin zone and bonding on the right side. Figure 4 shows a *positive* MM overlap population throughout the zone. The total overlap population averaged over the entire zone is 0.165. For comparison we calculated a hypothetical stacked aggregate of planar d^8 ML_4 fragments, type **4**, with stoichiometry $[RuCl_4^{4-}]_\infty$. The Ru–Ru overlap population for such a polymer is 0.031 (staggered) and 0.029 (eclipsed).

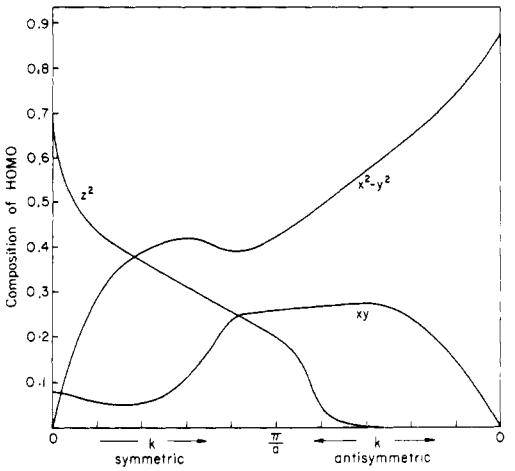

Figure 3. The composition of the HOMO of a d^8 $[RuCl_3^-]_\infty$ polymer as a function of k. Note the change from predominant z^2 to x^2-y^2 character as one moves from left to right.

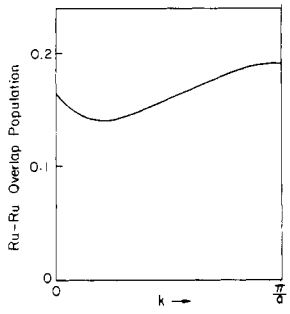

Figure 4. Total Ru–Ru overlap population in $[RuCl_3^-]_\infty$ as a function of k.

Table I. Extended Hückel Parameters

atom, orbital	H_{ii}, eV	exponent[a]
Ru, 5s	−8.31	2.078
5p	−3.28	2.043
4d	−10.74	5.378 (0.5340), 2.303 (0.6365)
Rh, 5s	−9.01	2.135
5p	−4.53	2.099
4d	−12.73	5.542 (0.5563), 2.398 (0.6119)

[a] Coefficients of double-ζ expansion in parentheses.

In summary: the simplified model of band formation from a_1 and b_2 fragment levels is sufficiently perturbed through orbital mixings that metal–metal σ bonding throughout the fourth d band occurs. The localized σ-bond model is a good starting point for an analysis of the bonding in the polymer.

How can one stabilize the hypothetical ML_2X chain? More bonding can be achieved by having the a_1 as low as possible, so that it contributes most to the left hand of the zone. This could be accomplished by having poorer σ donors as axial ligands, since these would then destabilize less the z^2 component of a_1. This point was confirmed by model calculations with axial hydride ligands whose Coulomb integral was varied.

In conclusion we have presented an argument for the existence of an ML_2X chain which can satisfy a low oxidation state d^8 metals' predilection for an angular fragment geometry, while providing an alternative to simple trimerization of ML_4. The discussion of the band structure of such a hypothetical material has been most instructive—it shows how the orbitals of a polymer can be assembled from many different starting points, and it

(5) See: Whangbo, M.-H.; Hoffmann, R.; Woodward, R. B. *Proc. R. Soc. London, Ser. A* **1979**, *A366*, 23–46 and references therein.

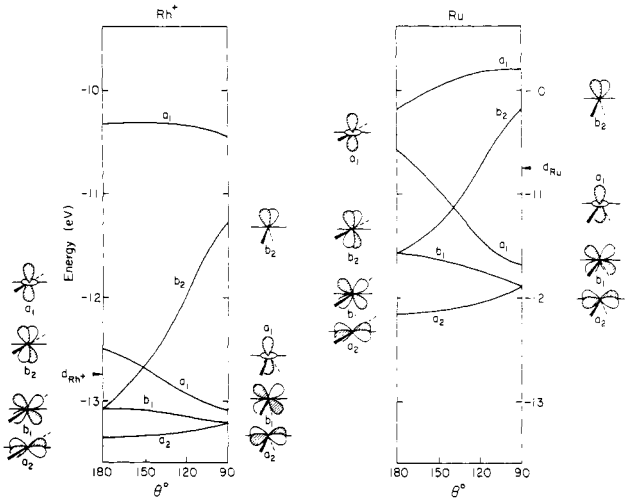

Figure 5. Walsh diagrams for the square-planar (θ = 180°) to angular (θ = 90°) deformation in $Ru(CO)_4$ (right) and $Rh(CO)_4^+$ (left).

illustrates the utility and relationship of localized and delocalized perspectives.

Acknowledgment. This work was prompted by the visit of H. B. Gray to Cornell as a Baker Lecturer. We are grateful to the National Science Foundation for its support of this research through Grant CHE 7828048 and also through DMR Grant 7681083 to the Materials Science Center at Cornell University. The permanent address of C. Minot is the Laboratoire de Chimie Théorique, Bat. 490, Université de Paris-Sud, Orsay, and we are grateful to the CNRS and the U.S.–France Exchange Program of the National Science Foundation for the support of his stay at Cornell.

Appendix: Why Do Some ML_4 Fragments Prefer Angular and Some Flat Geometries?

For a d^8 configuration, low oxidation states, e.g., Fe(0), Ru(0), Os(0), clearly favor the angular fragment in **1** in complexes, whereas high oxidation state metals, e.g., Ni(II), Pd(II), Pt(II), prefer the flat square-planar geometry **2**. All this is for low-spin complexes. Why is this so?

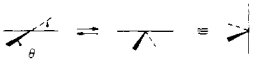

2 1

A model calculation on $Ru(CO)_4$ vs. $Rh(CO)_4^+$ is instructive. The extended Hückel parameters for the metals are shown in Table I. These were obtained from a charge-iteration scheme following Basch, Viste, and Gray.[6] Not surprisingly the Coulomb integrals are all more negative for the more electronegative Rh^+.

The Walsh diagrams for the two ML_4 systems are shown side-by-side in Figure 5. It should be noted that in the Appendix we are using a different coordinate system (**25**) from that utilized in the body of the paper (**26**). The reasons for this are clear—there is a different natural choice of z axis in the two cases: The angle

25 Appendix 26 In paper

varied, θ, is between two trans ligands. The general features of the orbitals at either extreme are well known.[4] Among the d orbitals xy transforms as a_2, xz as b_1, yz as b_2, and z^2 and x^2-y^2 as a_1. The angular fragment has the familiar pattern of three below two, the two being the a_1 and b_2 hybrids we discussed earlier. The square-planar geometry also has four orbitals at lower energy. One of them, the a_1 z^2 is stabilized by θ decreasing from 180°, due to loss of some equatorial σ antibonding. The effect is of similar magnitude for Ru as for Rh^+.

The difference between Ru and Rh^+ clearly can be traced to the b_2 rises in both cases. There are two reasons for this: (1) σ antibonding is turned on, there is none for θ = 180°, **27**, and (2) in the case of the carbonyl, π bonding is lost. The first effect

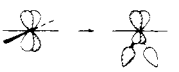

27

is the most important. The σ antibonding that is turned on is greater for the Rh^+ case simply because the Rh^+ levels are at lower energy, closer in energy to the donor levels they interact with, as one departs from the square-planar geometry. Thus both a more electronegative metal and better σ-donor ligand should favor the square-square or flat geometry over the angular alternative.

(6) Basch, H.; Viste, A.; Gray, H. B. *Theor. Chim. Acta* **1967**, *3*, 458.